5-2024

The Impact of Stable Modes on Saturation in Magnetorotational Turbulence

Hongke Lu
Bates College, hlu@bates.edu

The Impact of Stable Modes on Saturation in Magnetorotational Turbulence

Hongke Lu

Department of Physics and Astronomy, Bates College, Lewiston, ME 04240

The Impact of Stable Modes on Saturation in Magnetorotational Turbulence

An Honors Thesis

Presented to the Department of Physics and Astronomy

Bates College

in partial fulfillment of the requirements for the

Degree of Bachelor of Science

by

Hongke Lu

Lewiston, Maine

April 1, 2024

Contents

List of Figures

Acknowledgments

I would like to thank my mom, dad, and all my family members for their efforts to give me the opportunity to study at Bates College. Thanks to my advisor, Professor Jeffrey S. Oishi, for introducing me to the area of plasma physics and guiding me to complete this interesting project. I also want to thank all the physics faculty, especially Professor Aleksandar M. Diamond-Stanic, Professor Hong Lin, Professor Wesley C. Gillis, and Professor Nathan E. Lundblad for their help and guidance along my undergraduate years.

Abstract

The magnetorotational instability (MRI) plays a pivotal role in the dynamics of protoplanetary disks and the accretion processes near black holes in galactic nuclei. MRI drives turbulence that transports density, heat, and angular momentum in the accretion disk. In ideal MRI, each unstable mode has a corresponding conjugate stable mode with a similar absolute value of the growth rate. This thesis investigates local magnetorotational turbulence in a shearing box with a uniform magnetic field through 3D incompressible magnetohydrodynamic simulations. Utilizing the Dedalus framework, we formulate an eigenvalue problem for MRI, and found the fastest-growing mode and its conjugate stable mode, along with their mode structures. We observed that in the linear growth phase, the most unstable mode dominated the state vectors of the MRI simulation. Using eigenmode projection, we found that in the turbulence phase, stable modes are excited and contribute to the turbulence of MRI.

CHAPTER 1

Introduction

1. Magnetorotational Instability

As much as 99%, according to some estimates, of the observable universe is made up of plasma, or the fourth state of matter [1]. From fusion devices and Earth's ionosphere to the interstellar medium, plasma is everywhere. As a result, understanding the properties and behaviors of plasma under different conditions is fundamental to understanding a wide range of physical phenomena and technological applications.

Among these behaviors of plasma is magnetorotational instability (MRI), a fundamental process that plays a crucial role in astrophysical dynamics. The disks of dust and ionized gas, which are in plasma states [2], are found around massive celestial bodies like neutron stars and black holes [3][4]. These disks of dust and gas create an accretion motion under weak magnetic fields in the universe, and MRI is found to be a powerful model to explain the rapid transportation of angular momentum and mass in the disk, enabling us to simulate the evolution of celestial bodies. The canonical model of MRI is depicted in figure 1.1, where two masses are connected by a spring. Because of the gravity of the central object, the inner mass moves faster than the outer mass, resulting in the inner mass being pulled back while the outer mass is propelled forward. This dynamic leads to the outward transport of angular momentum. MRI was first formulated by Velikhov and Chandrasekhar in conducting liquid Couette flow [5][6], and not until about thirty years later did Balbus and Hawley identify MRI as a potential

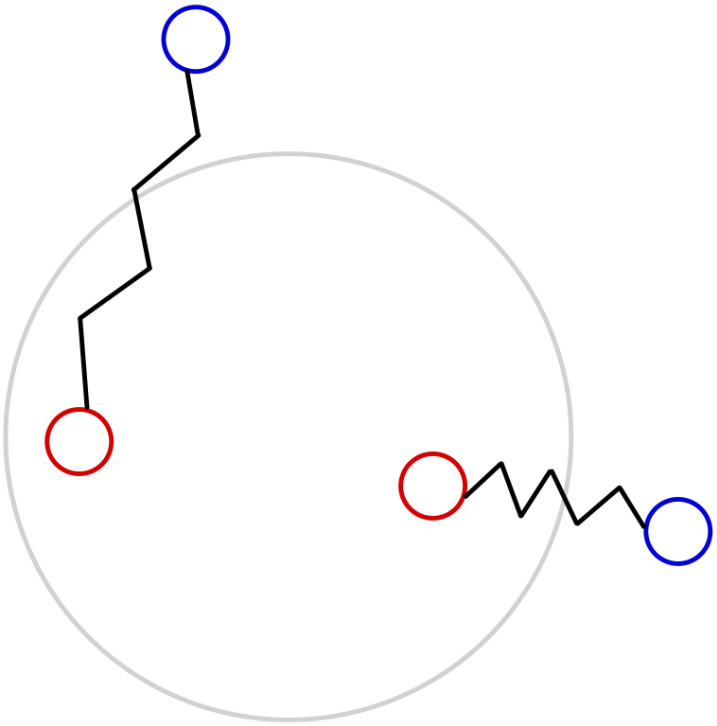

FIGURE 1.1. A canonical model of Magnetorotational Instability, with modeling the magnetic field as springs that connecting two masses.

mechanism for transporting angular momentum in astrophysical systems [7]. The advancements in our understanding of MRI have been remarkable, with recent decades witnessing significant progress in numerical simulations [8][9][10][11]. These efforts have provided deeper insights into the mechanisms underlying MRI and its implications for astrophysical processes. A landmark achievement in this field was made by Wang and his colleagues, who obtained direct evidence of MRI's existence through experimental work conducted at the Princeton Plasma Physics Laboratory [12].

2. Conjugate Stable Mode

Astrophysicists have used analytical methods to solve and predict the linear growth phase of magnetorotational instability, yet the turbulence phase remains a vibrant area of research. Among the methods proposed to explain the saturation of energy in plasma flow, the excitation of conjugate stable modes is particularly notable due to its general behavior in plasma flows [13][14][15][16][17][18][19]. This stable mode excitation is first observed in collisionless trapped electron mode turbulence [13]. For local (quasihomogeneous) systems, when we solve a system of linearized partial differential equations, just like solving an equation with complex roots, in some case for every unstable mode there is a conjugate stable mode. During the linear phase, unstable modes grow exponentially while stable modes decay at a similar rate. However, in the nonlinear phase, energy transitions from unstable to stable modes via cross-term interactions. The concept of damped mode excitation, alongside these findings, has been explored both computationally and theoretically in various contexts. Furthermore, it has been confirmed through observations in dipole-confined plasma within laboratory experiments [20].

3. Our Approach

We investigate the impact of conjugate stable modes on the turbulence of magnetorotational instability (MRI). First, by formulating a rotating plane Couette flow under a weak magnetic field, we create a localized MRI scenario using the shearing box approximation [21]. Second, we study the linearized nondimensionalized magnetohydrodynamics equation to investigate the growth rate of the three dimensional MRI. We identified the maximum growing eigenmode and its conjugate stable eigenmode using the Dedalus Package [22]. This package also allows us to export the structure of the eigenmodes. Subsequently, we constructed an initial value problem,

or simulation, of the MRI turbulence. Then we performed eigenmode analysis by projecting the left-eigenmodes against the nonlinear simulation of MRI turbulence. This analysis enables us to determine the eigenmode amplitude for both the unstable mode and its conjugate stable mode.

CHAPTER 2

Methods

1. System Set-up

We study the 3D time evolution of incompressible magnetized rotating plane Couette (rPC) flow to investigate magnetorotational turbulence, as figure shown in 2.1. Taylor-Couette flow occurs in the gap between two concentric cylinders that can rotate independently of each other. By taking the limit as the radius of the concentric cylinders approaches infinity, the curvature of the cylinder effectively becomes zero. Assuming periodic boundary conditions around the circumference, we can establish a rotating plane Couette flow. We express the incompressible rotating plane Couette flow using a set of partial differential equations, where $\mathbf{u}$ denotes the three-dimensional velocity field, and P denotes the scalar pressure field.

$$\partial_t \mathbf{u} + \mathbf{u} \cdot \nabla \mathbf{u} = -\frac{1}{\rho}\nabla P - 2\mathbf{\Omega} \times \mathbf{u} + \nu \nabla^2 \mathbf{u} \tag{2.1}$$

$$\nabla \cdot \mathbf{u} = 0 \tag{2.2}$$

In the equations above, ν is the fluid viscosity and Ω is the rotation rate. Then we apply a magnetic field to our system. We assume the charged particle move with the fluid element, therefore the moving charge will create an induced magnetic field. Thus we can add the induced magnetic field components to our system of differential equations. We use vector potential $\mathbf{A}$ to enforce the condition where $\nabla \cdot \mathbf{B} = 0$, and $\mathbf{A}$ is defined as $\mathbf{B} = \nabla \times (\mathbf{A} + \nabla\phi)$. $\mathbf{J}$ is volume current density and $\mathbf{J} = \nabla \times \mathbf{B}$. As a result, the complete system of partial differential equations

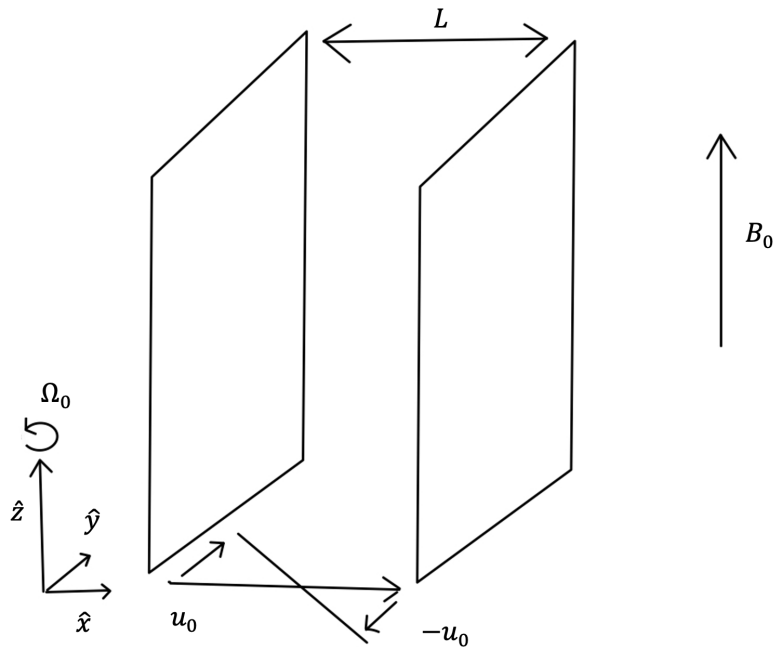

FIGURE 2.1. Diagram of our set-up, an rotating plane Couette flow with initial magnetic field B_0. Our system is a cube where the side length is L. The background flow drives by rotating planes each plane with velocity of u_0 and the whole system is rotating with rotation rate Ω_0. Then we exert an weak magnetic field B_0.

is:

$$\partial_t \mathbf{u} + \mathbf{u} \cdot \nabla \mathbf{u} = -\frac{1}{\rho}\nabla P + \mathbf{J} \times \mathbf{B} - 2\boldsymbol{\Omega} \times \mathbf{u} + \nu \nabla^2 \mathbf{u} \tag{2.3}$$

$$\nabla \cdot \mathbf{u} = 0 \tag{2.4}$$

$$\partial_t \mathbf{A} = \mathbf{u} \times \mathbf{B} + \eta \nabla^2 \mathbf{A} + \nabla \phi \tag{2.5}$$

$$\nabla \cdot \mathbf{A} = 0 \tag{2.6}$$

Where η is resistivity of the charged fluid and ϕ is the electric potential.

We can then nondimensionalized our system of partial differential equations by dividing each term by $\frac{T^2}{L}$, where T is characteristic time scale and L is characteristic length, then every terms become unitless, including parameters ν, Ω, η become unitless parameters, and velocity

field, magnetic field, vector potential, volume current density all become unitless vectors. The system of partial differential equation become:

$$\partial_{t_*}\mathbf{u}_* + \mathbf{u}_* \cdot \nabla \mathbf{u}_* = -\nabla P_* + Co\mathbf{J}_* \times \mathbf{B}_* - 2\boldsymbol{\Omega} \times \mathbf{u}_* + \frac{1}{Re}\nabla^2 \mathbf{u}_* \tag{2.7}$$

$$\nabla \cdot \mathbf{u}_* = 0 \tag{2.8}$$

$$\partial_t \mathbf{A}_* = \mathbf{u}_* \times \mathbf{B}_* + \frac{1}{Rm}\nabla^2 \mathbf{A}_* + \nabla \phi_* \tag{2.9}$$

$$\nabla \cdot \mathbf{A}_* = 0 \tag{2.10}$$

Where $Co \equiv \frac{2v_A^2}{\Omega^2 L^2}$ is the Cowling number and $v_A^2 \equiv B_0^2/\rho$ is the square of the Alfvén speed, $Re \equiv \frac{\mathbf{u_0}L}{\nu}$ is Reynolds number, a measurement of turbulence of the fluid , $Rm \equiv \frac{\mathbf{u_0}L}{\nu}$ is the magnetic Reynolds number, a measurement of the resistivity of the fluid. Variable $\mathbf{u}_*$, $\mathbf{B}_*$, $\mathbf{A}_*$, etc represents nondimensionalized quantities.

2. Linear Growth Rate

We perturb all the vectors in all three dimensions to solve for the linear growth rate for MRI. In order to do this, we write $\mathbf{u}$ as $\mathbf{u_0} + \mathbf{u_1}$, $\mathbf{B}$ as $\mathbf{B_0} + \mathbf{B_1}$, $\mathbf{A}$ as $\mathbf{A_1}$, and $\mathbf{J}$ as $\mathbf{J_1}$ where $\mathbf{u_1}$, $\mathbf{B_1}$, $\mathbf{A_1}$, and $\mathbf{J_1}$ are some infinitesimal perturbation to our system. Thus we can expend our system of partial differential equations as:

$$\partial_{t_*}\mathbf{u_1} + \mathbf{u_0} \cdot \nabla \mathbf{u_1} + \mathbf{u_1} \cdot \nabla \mathbf{u_0} - Co\mathbf{J_1} \times \mathbf{B_0} \tag{2.11}$$

$$-2\boldsymbol{\Omega_0} \times \mathbf{u_1} - \frac{1}{Re}\nabla^2 \mathbf{u_1} + \nabla P_1 = -\mathbf{u_1} \cdot \nabla \mathbf{u_1} + Co\mathbf{J_1} \times \mathbf{B_1} \tag{2.12}$$

$$\nabla \cdot \mathbf{u_1} = 0 \tag{2.13}$$

$$\partial_{t_*}\mathbf{A_1} - \frac{1}{Rm}\nabla^2 \mathbf{A_1} - \mathbf{u_1} \times \mathbf{B_0} - \mathbf{u_0} \times \mathbf{B_1} + \nabla \phi_1 = \mathbf{u_0} \times \mathbf{B_0} + \mathbf{u_1} \times \mathbf{B_1} \tag{2.14}$$

$$\nabla \cdot \mathbf{A_1} = 0 \tag{2.15}$$

We intentionally write the equation above in the form of $\mathcal{M} \cdot \partial_t \mathbf{X} + \mathcal{L} \cdot \mathbf{X} = \mathbf{F}(\mathcal{X}, t)$, Where $\mathcal{M}$ and $\mathcal{L}$ are matrices of linear differential operators, and $\mathcal{X}$ is the state vectors where in our case are vectors $\mathbf{u}_*$, $\mathbf{A}_*$,P_*, and ϕ_*. For Keplerian motion, defined by the rotation of particles

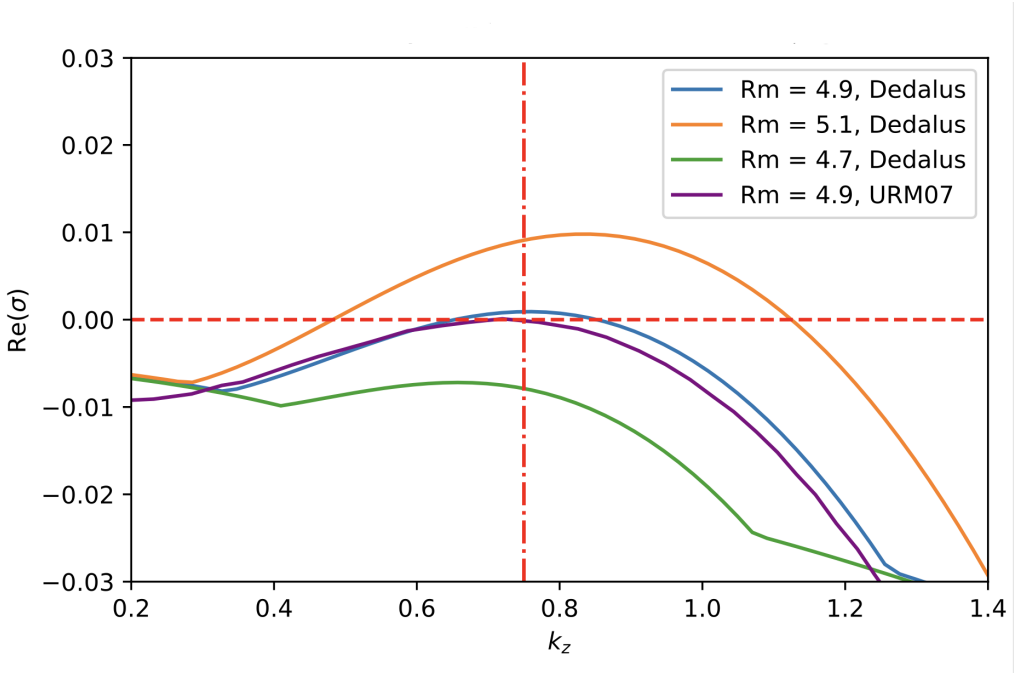

FIGURE 2.2. MRI growth rate, compared with result from Dedalus three dimensional eigenvalue problem and Umurhan et al [23]. The red line denotes the $K_z = 0.75$ and Re(σ)= 0 where the maximum growth rate occurs with critical parameters that make the MRI stable, or the maximum growth rate is 0.

in a disk around a central mass according to Kepler's laws, angular velocity Ω is purely a function of r, and follows a power law characterized by $q \equiv -\frac{\ln \Omega}{\ln r} = \frac{3}{2}$ where r is the radius to the center of rotational motion and Ω is rotational rate. Then we define the background flow as $\mathbf{u_0} = -q\Omega_0 x\hat{y}$. We then build our system in Dedalus using a Chebyshev basis in x direction, since we are solving the mode structure in x. We assume our system is periodic in y and z directions, so using a Fourier basis in y and z direction. Then we add our boundary conditions that we assume perfect conductor boundary for the magnetic field and non-slip boundary conditions on the velocity field. Together we have the boundary condition for ideal MRI as $\mathbf{u} = \mathbf{A_y} = \mathbf{A_z} = \phi = 0$ at the boundary $x = \pm\frac{L_x}{2}$.

We verify our system set-up with comparison with the critical parameters for Rm, Re, and Co listed in Umurhan et al [23], and we found the same parameters with uncertainty less than the last significant digit.

3. Dedalus Implementation

3.1. Eigenvalue Problem. Dedalus is an open source python package that solve partial differential equations using spectral method. Required by Dedalus, in order to spatially resolve the change in x direction, as we mentioned in the previous section, we built Chebyshev basis to solve for the system in x. Then we create our system with the domain of $L_y \times L_z \times L_x = 2\pi/k_y \times 2\pi/k_z \times 1$, where k_y and k_z are the Fourier modes $\exp(ik_y y)$ and $\exp(ik_z z)$. Therefore, by solving across a range of ky and kz values, we can identify the specific ky and kz associated with the most unstable mode. In this thesis, simulations are in the size of $N_y \times N_z \times Nx = 64 \times 64 \times 128$ and we verified that the system will be fully resolved under these resolution. We assume the perturbation in y direction is constant, implying $k_y = 0$. We solve the partial differential equation using separation of variable and we can then formulate our eigenvalue problem with eigenvalue σ for $\mathbf{u}$ as below:

$$\mathbf{u} = \sum_{k_z} \hat{\mathbf{u}}(x) \exp(\sigma t + ik_z z) \tag{2.16}$$

The result of the critical parameters of MRI is shown in figure 2.2. We then the eigenvalue problem with $Pm = 1$ and $Rm = 40Rm_c$ where $Rm_c = 4.9$. Then we have the growth rate plot shown in figure 2.3

3.2. Initial Value Problem. In order to simulate the magnetorotational turbulence, we use Dedalus IVP or initial value problem feature to implement our numerical simulation. We use the same problem setting as the eigenvalue problem except that we build our system using real number instead of complex number. We then give the initial condition of random noise to our system as the perturbation.

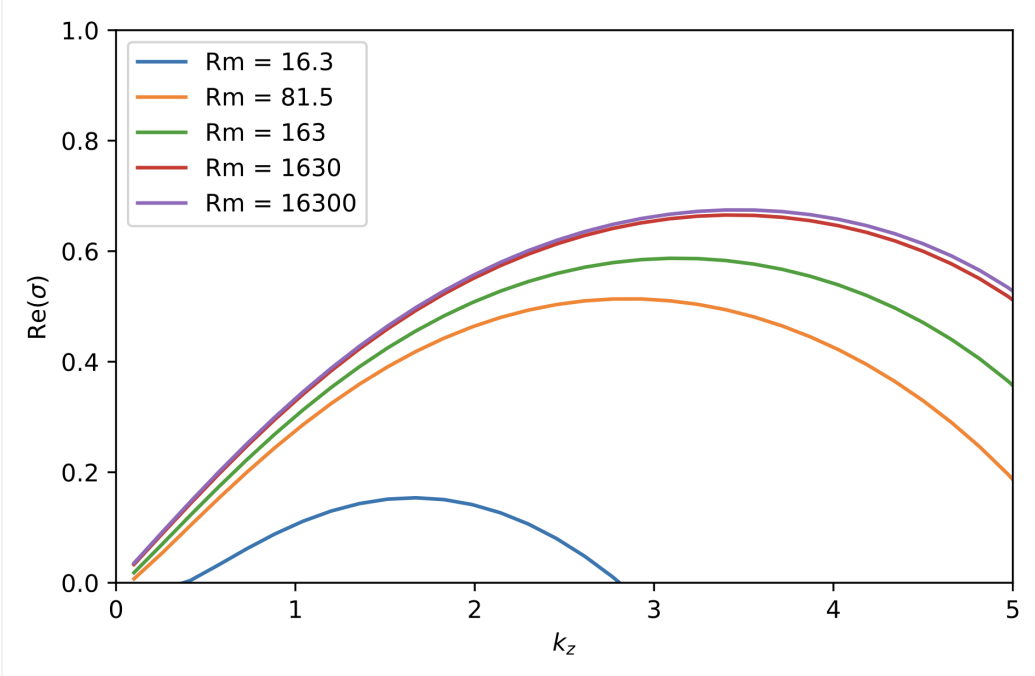

FIGURE 2.3. The growth rate of the max growing mode of MRI for various different Rm, and we keep $Pm = 1$, $Co = 0.08$.

CHAPTER 3

Analysis

1. Eigenmode Structure

After we formulated the system of differential equation into an eigenvalue problem, similar to solving the eigenvalue and eigenvector for an matrix, we will get the eigenvalue with their corresponding eigenvector or namely eigenmode. While we are solving for the most unstable mode in the section above, there also exist an conjugate stable mode for the most unstable mode. We use the solve_dense function in Dedalus to solve for all the eigenvalues. After we filtered out all the eigenvalues that are infinite, we plot part of the eigenvalues as shown in plot 3.1. We plot vector **u** and **A** vectors respect to the x axis. The real and imaginary part of

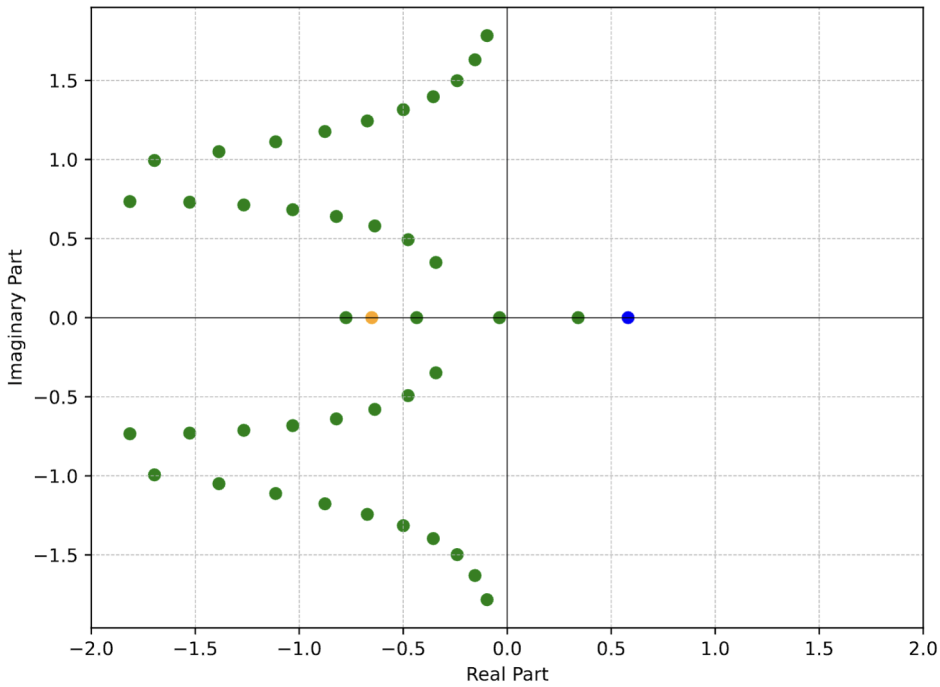

FIGURE 3.1. Plot of eigenvalues in the real and complex plane. The blue point is the most unstable mode with growth rate of 0.58, and the yellow point is the conjugate stable mode with growth rate of -0.67. All the other mode are marked in green

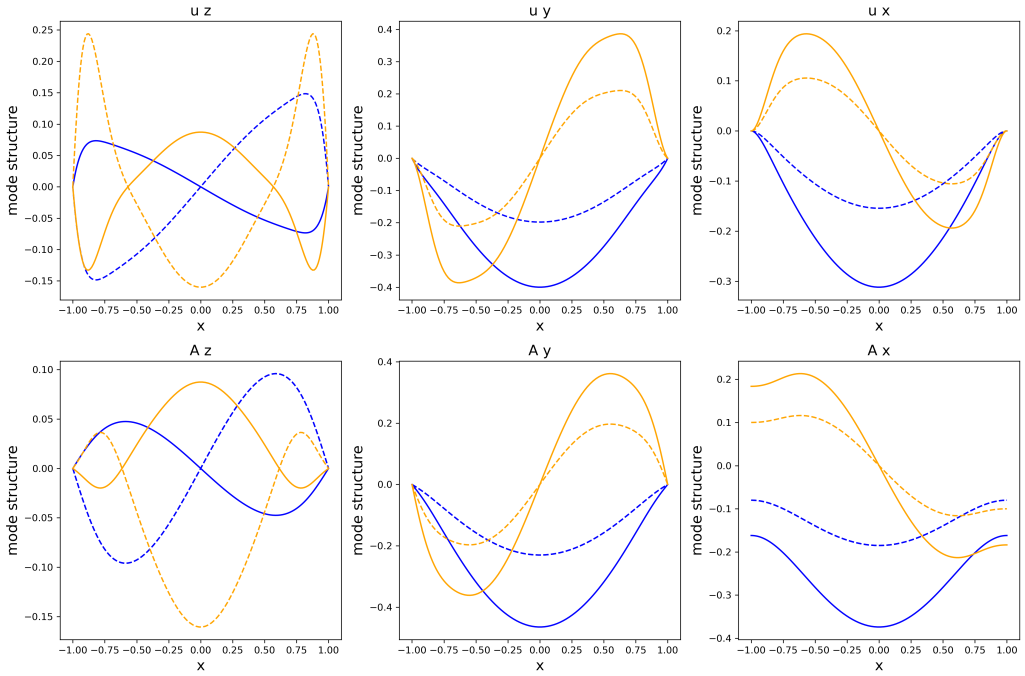

FIGURE 3.2. Plot of eigenmode structure of the most unstable mode and its conjugate stable mode. The blue lines denote the most unstable mode where growth rate is 0.58 and the orange lines denote the conjugate stable mode where growth rate is 0.65. The solid lines and dash lines represent the real and imaginary part of the eigenmode respectively.

vectors **u** and **A** are shown in the figure 3.2. Since the our system is viscid, so the the stable and unstable mode are not only different in phase, but also different in structure. At the same time, in our case, because of the viscosity and resistivity the eigenvalue or the growth rate for the most unstable mode and its conjugate stable mode do not have same absolute value, our stable mode projection will be damped. As a result, we will refer to We are going to continue working on the ideal inviscid MRI to further elaborate this project. We also plotted the real part of the unstable mode and its conjugate unstable mode in two dimension, as shown in figure 3.4, and figure 3.3. In general they looks similar except there is a phase shift between the most unstable and conjugate stable mode.

2. Energy Evolution

While analyzing our simulation, the first thing is to verify our simulation with the maximum growth rate we discovered in the previous section. For each step of our simulation, we record

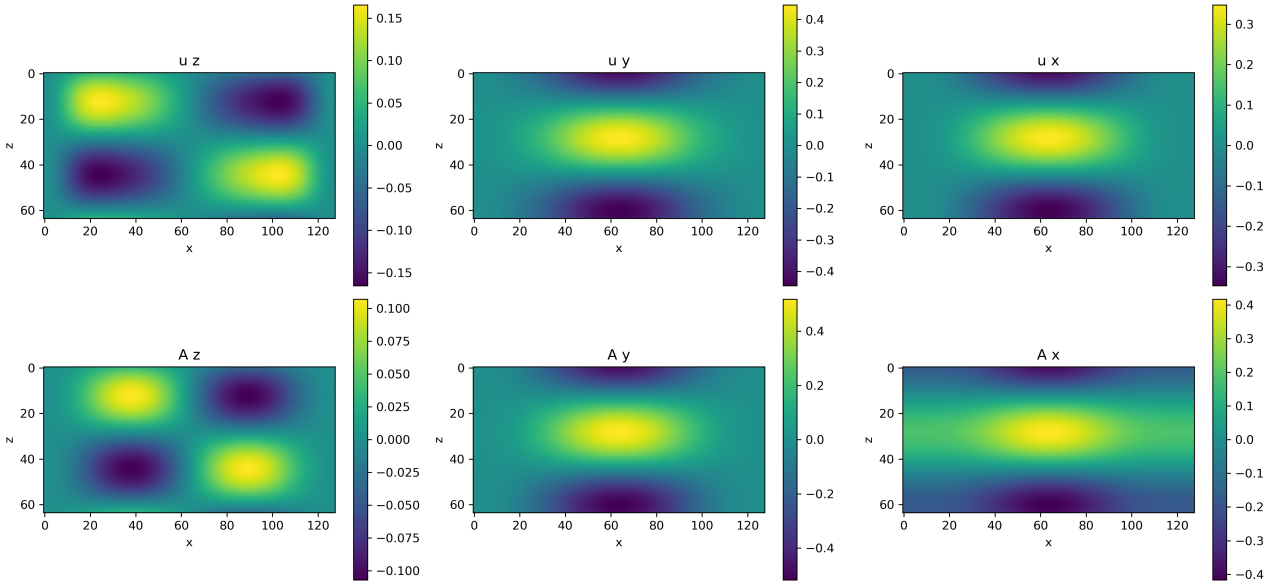

FIGURE 3.3. Plot of eigenvectors of the most unstable mode in two dimension.

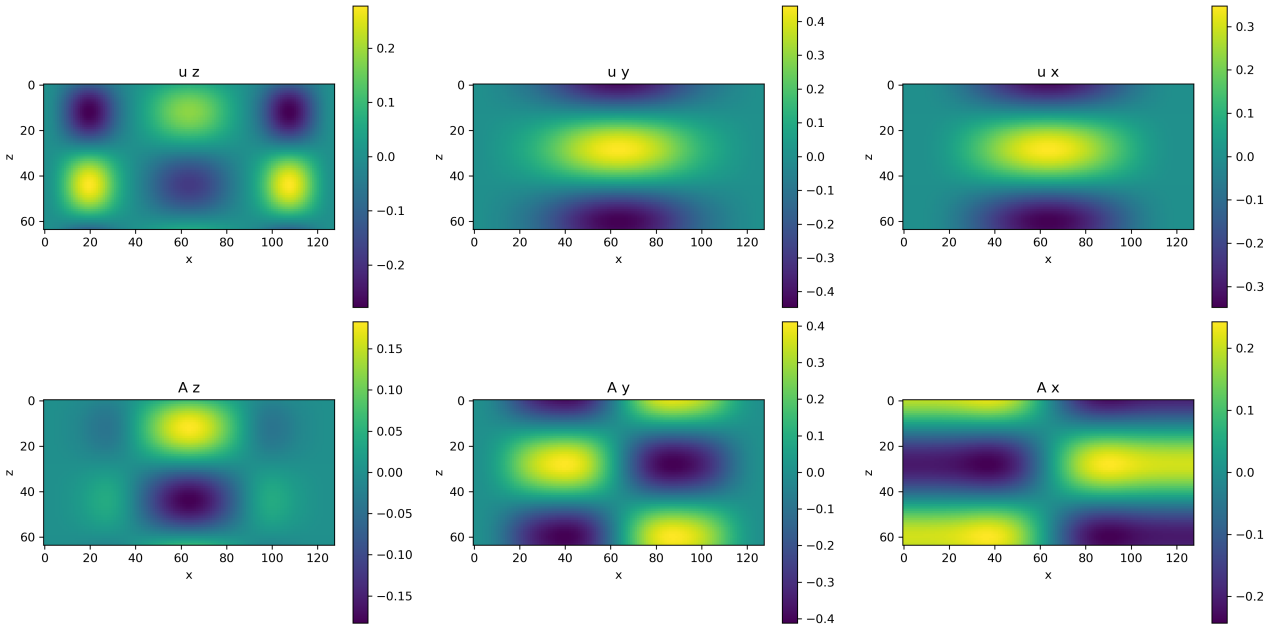

FIGURE 3.4. Plot of eigenvectors of conjugate stable mode of the most unstable in two dimension.

the root-mean-square velocity (V_{rms})of the field, which have the same unit as the velocity field, and therefore should follows the growth rate we calculated in the eigenvalue problem. Recall the velocity field is in the form of:

$$\mathbf{u} = \hat{\mathbf{u}}(x)\exp(\sigma t + ik_z z) \tag{3.1}$$

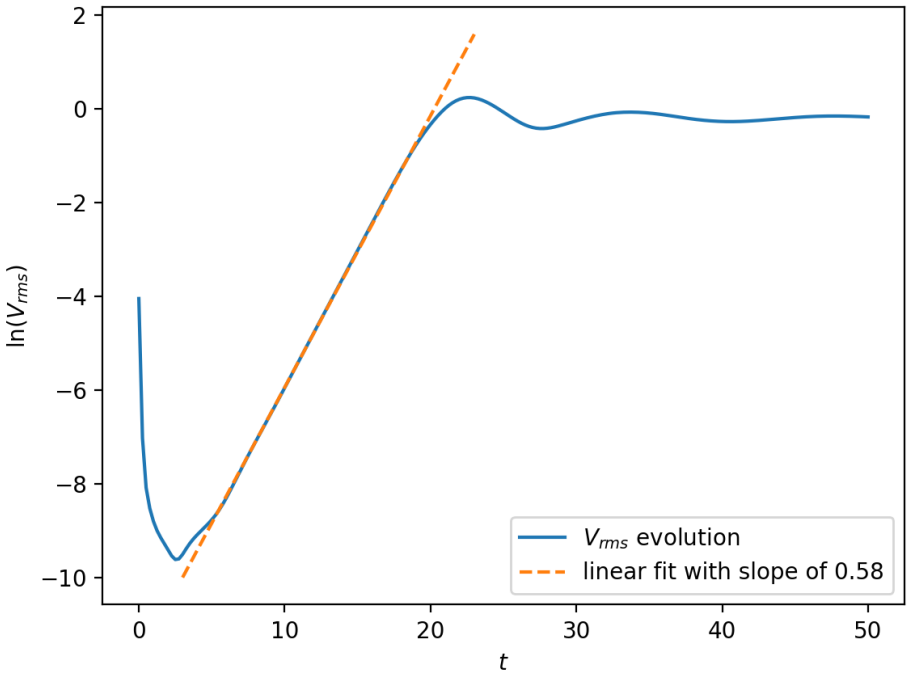

FIGURE 3.5. Evolution of V_{rms} respect to time. The orange dashed line is the linear fit to the linear growing phase of the MRI simulation. The result from linear fit agreed with the max growth rate calculation from Chapter 2.

Which means the unstable mode should grow exponentially. While the system in the linear growing phase, the stable mode will decay exponentially. However, since the initial condition is small, the stable mode will approach zero, and the most unstable mode will dominant V_{rms}. Figure 3.5 is what we observed in the evolution of the V_{rms}. The energy evolution of MRI is similar to the V_{rms} evolution. We calculate the magnetic energy and kinetic energy as below:

$$ME = \int \mathbf{B} \cdot \mathbf{B} dV \tag{3.2}$$

$$KE = \int \mathbf{u} \cdot \mathbf{u} dV \tag{3.3}$$

And the total energy will be simply be $KE + ME$. As shown in figure 3.6 energy start to saturate after $t = 20$ and evolution energy are similar across total energy, KE, and ME. It is also clear in figure 3.7 that all the energy experienced similar growth rate in the linear growing phase. We are particular interest in the saturation of MRI and we will use eigenmode projection

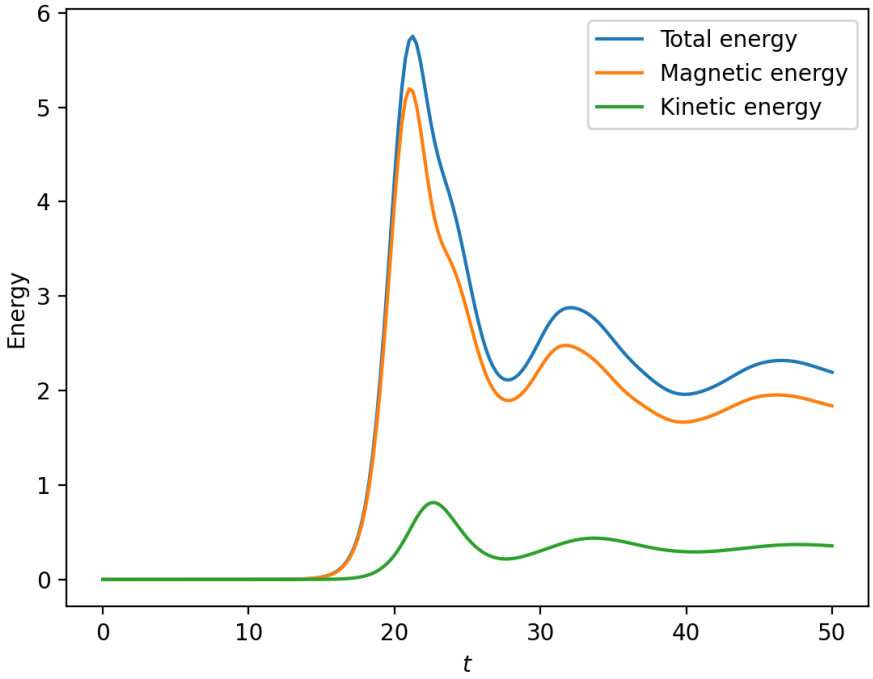

FIGURE 3.6. Evolution of total energy, magnetic energy and kinetic energy respect to time in linear scale. The energy starts to saturate around $t = 20$.

to identify the contribution of particular eigenmode in the magnetorotational turbulence in the next section.

3. Left Eigenmode

To solve for the maximum growth rate, we formulated the system of partial differential equation into an eigenvalue problem, and we calculated the eigenvalue, which is the growth rate, and the corresponding eigenvector, or eigenmode. Mathematically we solve a eigenvalue problem that can be described as:

$$\lambda M \cdot X + L \cdot X = 0 \tag{3.4}$$

Where λ is the eigenvalue, X is state vectors, and M and L are some linear operators. Dedalus then solved the eigenvalue problem to find λ_i and X_i with sparse matrix representation of M

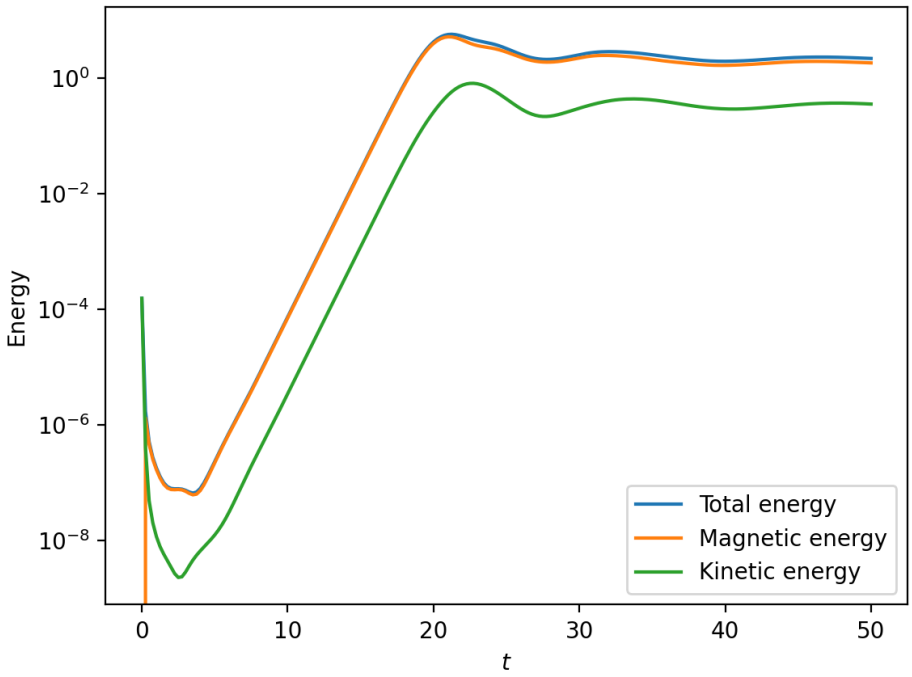

FIGURE 3.7. Evolution of total energy, magnetic energy and kinetic energy respect to time in $\log_{10}$ scale. The magnetic energy start from 0 since the inital condition is 0 in **A**.

and L [22], which satisfies:

$$\lambda_i M \cdot X_i + L \cdot X_i = 0 \tag{3.5}$$

Where λ_i is eigenvalue and X_i is their corresponding eigenvectors. All the eigenvectors together construct a complete basis to represent the information in the linear operators. Since we are discrete our system with resolution of $N_y \times N_z \times N_x = 64 \times 64 \times 128$ most of eigenvalue and eigenvectors are useless and we are only looking for the most unstable mode and its conjugate stable mode.

The left eigenvectors Y_i are defined as:

$$\lambda_i Y_i^* \cdot M + Y_i^* \cdot L = 0 \tag{3.6}$$

And the left and right eigenvectors are orthonormal to each other, and in Dedalus, we can set left and right eigenvector to be orthnormal to each other, meaning:

$$Y_i^* \cdot M \cdot X_j = \delta_{i,j} \tag{3.7}$$

Where $\delta_{i,j}$ is the Dirac delta function. We can then call the $Y_i^* \cdot M$ to be the modified left eigenvectors. We solved the left eigenmode using Dedalus, codes are available in the link in the appendix.

4. Eigenmode Projection

We solved the eigenvalue problem to get a basis to describe our time dependent nonlinear evolution of MRI. The basis will be complete if we solve the eigenvalue problem for all k_z , but it is not realistic. We picked the k_z that corresponding to the most unstable mode, namely to find the k_z that corresponding to the maximum growth rate in figure 2.3 .For each value of k_z there will be a set of eigenvalue and eigenvectors depend on spatial resolution that you choose for x, and in our case $N_x = 128$. And since there are eight variables in total (three from velocity field, three from vector potential, one for pressure, and one for electric potential), we will have $8 \times 128 = 1024$ set of eigenvalue and eigenvector pair (since we also have six τ terms to help us exert boundary conditions and four of them have two basis, we have 1036 pairs). As we described in section 1, most of the eigenvalue and eigenmode pairs are useless. And as we described in section 3, all the eigenmodes are linear independent of each other, since their inner product are 0 except the left and right eigenmode have the same index. Then we can write an arbitrary frame of the simulation as a summation of all the eigenmode with their weight [24].

$$f(t) = \sum_{k_z} \sum_{j=1}^{N_{ev}} \beta_j(k_z, t) \hat{f}_j e^{ik_z z} \tag{3.8}$$

In the arbitrary frame, the time dependent state vectors $f(t)$ can be break up in to a sum over all the k_z and sum over all the index of the eigenvalues, N_{ev}, then for each eigenmode $\hat{f}_j$ it have a corresponding eigenmode amplitude β_j . We approach the eigenmode projection method using Dedalus vector fields where Dedalus enabled conversion between grid space to coefficient space.

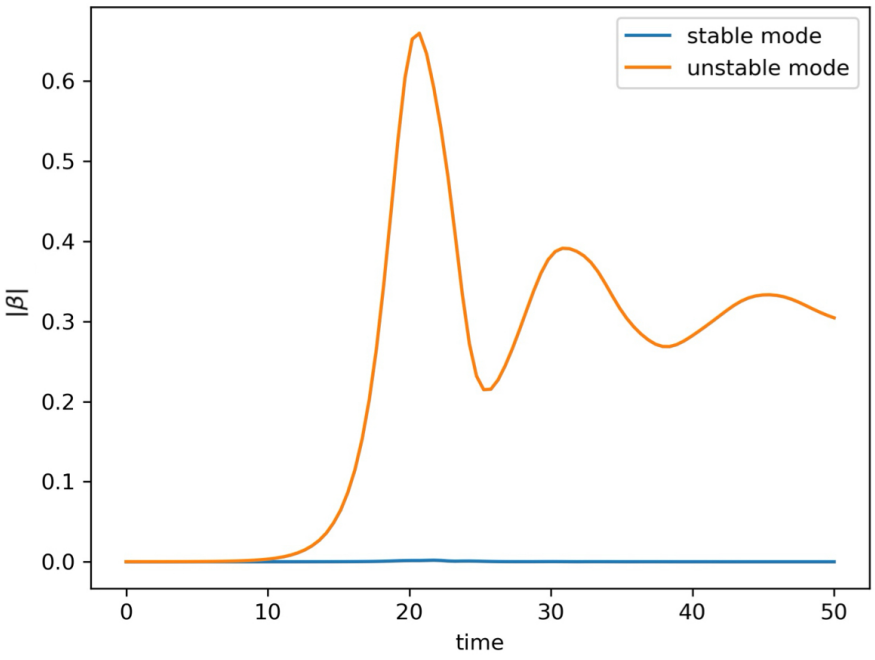

FIGURE 3.8. Evolution of $|\beta|$ of the most unstable mode and the conjugate stable mode in linear scale.

Just like we can decompose a random periodic function using Fourier series, we can decompose a random function with arbitrary boundary conditions using Chebyshev series. Thus we can formulate the each state using a series of Fourier and Chebyshev functions. We can write the left eigenvector $|g\rangle$and right eigenvectors $|f\rangle$ as:

$$|f\rangle = \sum_n \hat{f}_n e^{ik_n x} = \sum_n \hat{f}_n |\phi_n\rangle \tag{3.9}$$

$$|g\rangle = \sum_m \hat{g}_m e^{ik_m x} = \sum_m \hat{g}_m |\phi_m\rangle \tag{3.10}$$

Where $|\phi\rangle$ represents Fourier series in this case, but it can also represent any series of orthogonal polynomials. As we know that the left and right eigenvectors formed a Dirac delta function as 3.7 shown, or in this case $\langle g|f\rangle = 1$ if $m = n$. The right eigenvectors forms a complete basis for our state vectors in the simulation. As a result, we can implement the eigenmode projection to

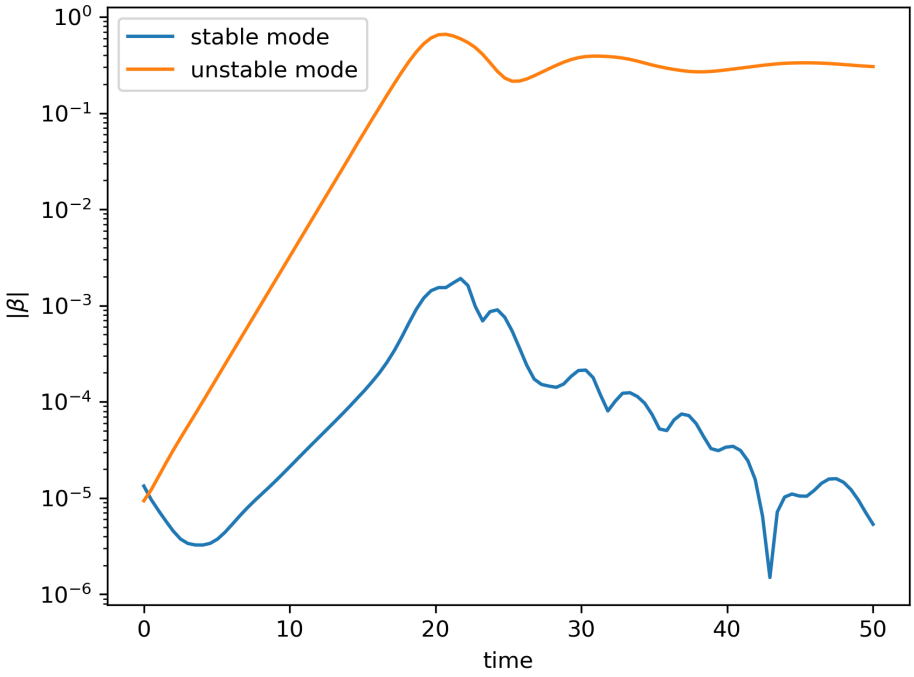

FIGURE 3.9. Evolution of $|\beta|$ of the most unstable mode and the conjugate stable mode in log scale.

calculate β with similar procedure.

$$\langle g|f(t)\rangle = \left(\sum_m \langle\phi_m|\,\hat{g}^\dagger\right)\left(\sum_n \beta_n \hat{f}_n(t)\,|\phi_n\rangle\right) \tag{3.11}$$

$$= \sum_m \sum_n \hat{g}^\dagger \beta_n \hat{f}_n(t)\,\langle\phi_m|\phi_n\rangle \tag{3.12}$$

$$= \sum_n \beta_n \hat{g}^\dagger \hat{f}_n(t) \tag{3.13}$$

$$= \beta \tag{3.14}$$

Which means that doing inner product using integration in the grid space is equivalence to summing all the element-wise product in coefficient space. And since our simulations are in real space and the eigenmodes are in complex space, we need to take the absolute value of β for our eigenmode projection.

Figure 3.8 shows a linear plot of the $|\beta|$ for each step of the simulation. We can see that the conjugate stable mode was not really excited. However, in figure 3.9, it shows clearly that the

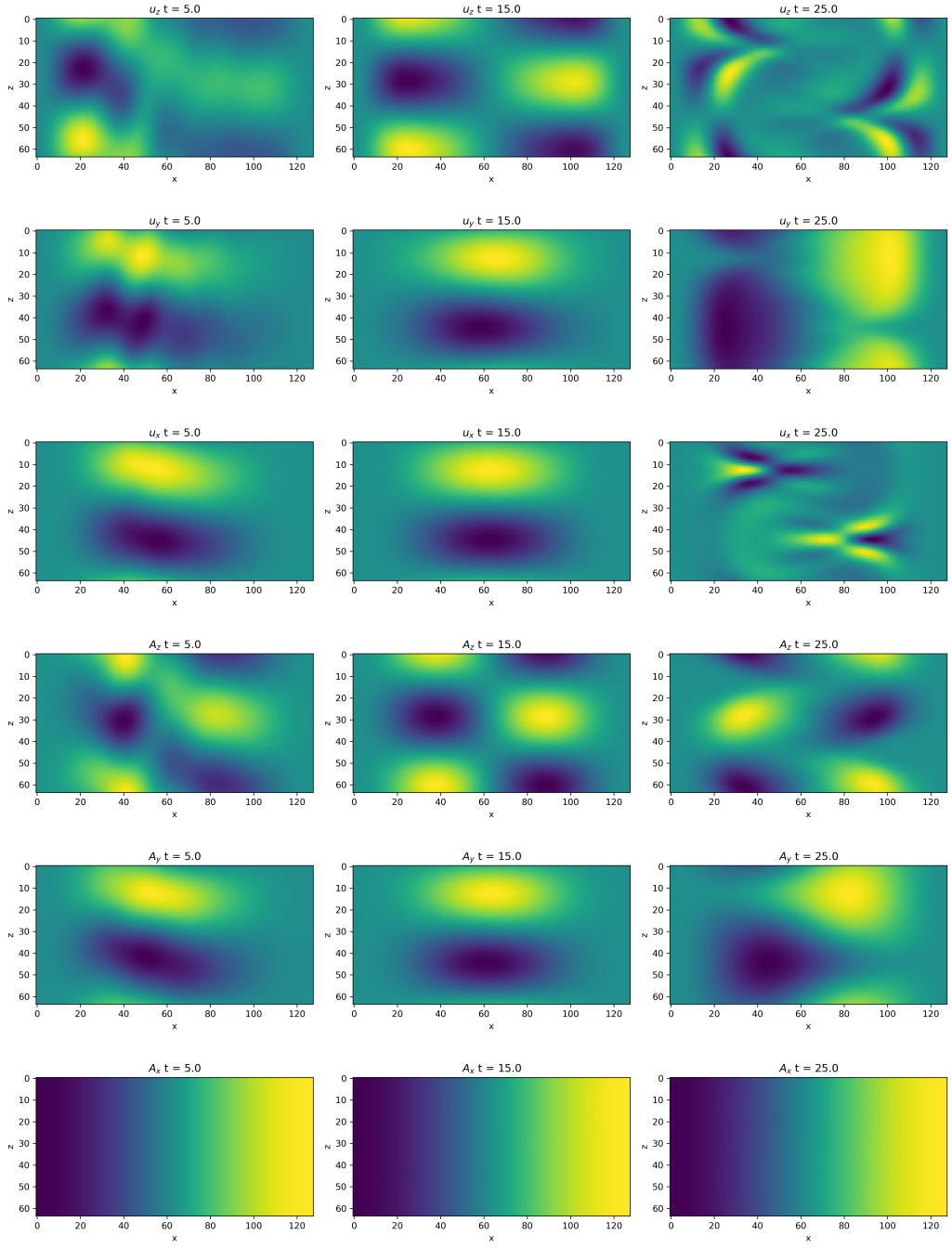

FIGURE 3.10. Two dimensional plot of the evolution of the state vectors **u** and **A** at t = 5, 15, and 25.

stable mode was excited but with very small amplitude. This is due to our basis are calculated in dissipated eigenmodes, meaning the resistivity term R_m and viscosity term R_e are not zero. In figure 3.10 , we can see clearly that in the linear growth phase the most unstable mode is

dominating the simulations. In the turbulence phase, we can see eigenmode excitation but they are still dominated by the most unstable mode.

CHAPTER 4

Summary and Conclusions

1. Summary and Conclusions

MRI is an important fluid instability in accretion disks around massive astrophysical bodies like black hole and neutron star. Understanding the evolution of eigenmodes over time lays the foundational work for studying angular momentum transport in MRIs. This thesis has developed and utilized a mix of analytical and numerical techniques to explore the saturation of MRI and the excitation of conjugate stable eigenmode. In the linear phase, the unstable modes will always grow exponentially and the stable modes will always decay exponentially. However, because of the nonlinear terms, the evolution of MRI saturated after a certain time step. In this thesis, we use eigenmode projection techniques and found the stable mode excitation and saturation of modes amplitude $|\beta|$ as a result of nonlinear terms appearing in the MRI systems.

2. Future work

In my thesis, the eigenmode have energy dissipation in itself due to the viscosity and resistivity in our problem set-up for the eigenvalue problem. As result of this problem set-up, the conjugate stable mode is excited but not a lot. We will look in the the ideal inviscid and resistance free problem set up to further elaborate this problem. We want to study the magnetorotational turbulence; however, due to limited time, we are not able to run large scale simulation with high Re and Rm. In our simulation after 50 time steps the turbulence stop. We want to run on larger clusters for longer time to better understand mode amplitude during turbulence. We are also interested in explore the implications of angular momentum transportation in the MRI, and how does it related to the eigenmode amplitudes.

Appendix A

Python code for formulation of eigenvalue problem and initial value problem, aka. simulation are available on https://github.com/jsoishi/mri_conjugate_modes

Bibliography

[1] Donald A Gurnett and Amitava Bhattacharjee. *Introduction to plasma physics: with space and laboratory applications*. Cambridge university press, 2005.

[2] Bruce T Draine. *Physics of the interstellar and intergalactic medium*, volume 19. Princeton University Press, 2010.

[3] Masayoshi Yokosawa and T Inui. Magnetorotational instability around a rotating black hole. *The Astrophysical Journal*, 631(2):1051, 2005.

[4] Daniel M Siegel, Riccardo Ciolfi, Abraham I Harte, and Luciano Rezzolla. Magnetorotational instability in relativistic hypermassive neutron stars. *Physical Review D*, 87(12):121302, 2013.

[5] E P Velikhov. Stability of an ideally conducting liquid flowing between rotating cylinders in a magnetic field. *Zhur. Eksptl'. i Teoret. Fiz.*, Vol: 36, 5 1959.

[6] S Chandrasekhar. The stability of non-dissipative couette flow in hydromagnetics. *Proceedings of the National Academy of Sciences*, 46(2):253–257, 1960.

[7] Steven A. Balbus and John F. Hawley. Instability, turbulence, and enhanced transport in accretion disks. *Rev. Mod. Phys.*, 70:1–53, Jan 1998.

[8] John F Hawley, Charles F Gammie, and Steven A Balbus. Local three-dimensional magnetohydrodynamic simulations of accretion disks. *Astrophysical Journal v. 440, p. 742*, 440:742, 1995.

[9] Robert A Piontek and Eve C Ostriker. Thermal and magnetorotational instability in the interstellar medium: two-dimensional numerical simulations. *The Astrophysical Journal*, 601(2):905, 2004.

[10] Wei Liu, Jeremy Goodman, and Hantao Ji. Simulations of magnetorotational instability in a magnetized couette flow. *The Astrophysical Journal*, 643(1):306, 2006.

[11] James M Stone, Kengo Tomida, Christopher J White, and Kyle G Felker. The athena++ adaptive mesh refinement framework: Design and magnetohydrodynamic solvers. *The Astrophysical Journal Supplement Series*, 249(1):4, 2020.

[12] Yin Wang, Erik P. Gilson, Fatima Ebrahimi, Jeremy Goodman, and Hantao Ji. Observation of axisymmetric standard magnetorotational instability in the laboratory. *Phys. Rev. Lett.*, 129:115001, Sep 2022.

[13] P. W. Terry, D. A. Baver, and Sangeeta Gupta. Role of stable eigenmodes in saturated local plasma turbulence. *Physics of Plasmas*, 13(2):022307, 02 2006.

[14] A. E. Fraser, P. W. Terry, E. G. Zweibel, and M. J. Pueschel. Coupling of damped and growing modes in unstable shear flow. *Physics of Plasmas*, 24(6):062304, June 2017.

[15] A. E. Fraser, P. W. Terry, E. G. Zweibel, M. J. Pueschel, and J. M. Schroeder. The impact of magnetic fields on momentum transport and saturation of shear-flow instability by stable modes. *Physics of Plasmas*, 28(2):022309, February 2021.

[16] Ping-Yu Li, M Pueschel, Paul Terry, and Garth Whelan. On the role of mode resonances in regulating zonal-flow-moderated plasma microturbulence. *Nuclear Fusion*, 63, 12 2022.

[17] B. Tripathi, P. Terry, A. Fraser, E. Zweibel, and M. Pueschel. Three-dimensional shear-flow instability saturation via stable modes. *Physics of Fluids*, 35, 10 2023.

[18] B. Tripathi, A. Fraser, P. Terry, E. Zweibel, M. Pueschel, and Evan Anders. Nonlinear mode coupling and energetics of driven magnetized shear-flow turbulence. *Physics of Plasmas*, 30, 07 2023.

[19] Taweesak Jitsuk, Alessandro Di Siena, M.J. Pueschel, P.W. Terry, F. Widmer, E. Poli, and J.S. Sarff. Global linear and nonlinear gyrokinetic simulations of tearing modes. *Nuclear Fusion*, 64, 02 2024.

[20] T. M. Qian and M. E. Mauel. Observation of weakly damped modes using high resolution measurement of turbulence in a dipole confined plasma. *Physics of Plasmas*, 27(1):014501, 01 2020.

[21] S A Balbus and J F Hawley. A powerful local shear instability in weakly magnetized disks. i - linear analysis. ii - nonlinear evolution. *Astrophysical Journal; (United States)*.

[22] Keaton J. Burns, Geoffrey M. Vasil, Jeffrey S. Oishi, Daniel Lecoanet, and Benjamin P. Brown. Dedalus: A flexible framework for numerical simulations with spectral methods. *Phys. Rev. Res.*, 2:023068, Apr 2020.

[23] O. M. Umurhan, O. Regev, and K. Menou. Nonlinear saturation of the magnetorotational instability near threshold in a thin-gap taylor-couette setup. *Phys. Rev. E*, 76:036310, Sep 2007.

[24] Adrian E. Fraser. *Role of Stable Eigenmodes in Shear-Flow Instability Saturation and Turbulence*. PhD thesis, 2020. Copyright - Database copyright ProQuest LLC; ProQuest does not claim copyright in the individual underlying works; Last updated - 2023-06-21.